Hindawi
Mathematical Problems in Engineering
Volume 2022, Article ID 4417418, 10 pages
https://doi.org/10.1155/2022/4417418

Research Article

Dynamics of Nanoplatelets in Mixed Convective Radiative Flow of Hybridized Nanofluid Mobilized by Variable Thermal Conditions

Iftikhar Ahmad,[1] Muhammad Faisal,[1] Qazi Zan-Ul-Abadin,[1] K. Loganathan,[2] Tariq Javed,[3] and Balachandra Pattanaik[4]

[1]*Department of Mathematics, Azad Jammu & Kashmir University, Muzaffarabad 13100, Pakistan*
[2]*Department of Mathematics & Statistics, Manipal University Jaipur, Rajasthan, India*
[3]*Department of Mathematics and Statistics, International Islamic University, Islamabad 44000, Pakistan*
[4]*Department of Electrical and Computer Engineering, College of Engineering and Technology, Wollega University, Nekemte, Ethiopia*

Correspondence should be addressed to Qazi Zan-Ul-Abadin; qazi.zain@ajku.edu.pk, K. Loganathan; loganathankaruppusamy304@gmail.com, and Balachandra Pattanaik; balapk1971@gmail.com

Received 18 July 2022; Revised 10 September 2022; Accepted 14 September 2022; Published 11 October 2022

Academic Editor: Waleed Adel

The present mathematical model discloses the effects of Boussinesq and Rosseland approximations on unsteady 3D dynamics of water-driven hybridized nanomaterial with the movements of nanoplatelets (molybdenum disulfide, MoS_2 and graphene oxide, GO). Variable thermal conditions, namely, VST (variable surface temperature) and VHF (variable heat flux), are opted to provide temperature to the surface. MHD effects have also been used additionally to make the study more versatile. In order to transmute the transportation equations into nondimensionlized forms, similarity transformations have been adopted. The Keller-Box technique has been applied to obtain a numerical simulation of the modeled problem. The convergence of the solution for both VST and VHF cases is presented via the grid independence tactic. Thermal setup against escalating choices of power indices and nonlinear thermal radiation parameter is discussed via graphical illustrations. The rate of heat transaction has been discussed with the growing choices of mixed convection, thermal radiation, and unsteady parameters through various tabular arrangements. It is observed through the present analysis that mixed convection parameter, radiation parameter, temperature maintaining indices (r, s), and unsteady parameter magnify the rate of heat transference under the control of platelet-shaped nanoparticles.

1. Introduction

In the last few years, the topic of nanofluids has become a major topic of research. Nanofluid designates a liquid suspension containing particles of diameter less than 100 nm. Makinde and Aziz [1] inspected the effect of convective-heating boundary constraints on nanoparticles. Mixed convection impact along with the steady dynamics of hybridized nanofluid is explored by Waini et al. [2] along a vertical surface. Gul et al. [3] premeditated the hybridized nanomaterial stirring on a dispersion sheet with the impression of magnetic dipole. Moreover, Waini et al. [4] conferred the effects of hybridized nanomaterial for heat transaction process for identical shear flow on a shrinking sheet. Forced convective heat transference of water conveying hybridized nanofluid Al_2O_3 and $Al_2O_3 - Cu$ with particle size 15 nm and 0.1% volume concentration was considered by Moghadassi et al. [5] and proposed that this model gives better results experimentally as compared to single phase tactic. Stagnation flow of $TiO_2 - Cu/H_2O$ hybridized nanofluid over an elongating obstacle with the induced magnetic field effect is incorporated by Ghadikolaei et al. [6]. Here, it was noticed that hybridized nanofluid proliferates heat transmission. Hybridized nanomaterial $Ag - MoS_2$ with base fluid $C_2H_6O_2 - H_2O$ over a prolonging obstacle is incorporated by Ali et al. [7] by considering activation energy aspects. Here, enhancement of thermal transference was the core objective of the reported work. The

thermal features of Williamson hybridized nanofluid (MoS_2 + ZnO) by considering engine oil as a base fluid are investigated by Yahya et al. [8] with the incorporation of heat source, thermal dissipation, and invariant magnetic field aspects. Heat transference in the stream of Maxwell hybridized ($GO - MoS_2$) nanofluid with the engine oil as a working liquid over a fluctuating vertical cylinder is addressed by Arif et al. [9]. The thermal performance of heat exchanger devices can be improved by the submersion of different shapes of nanoparticles into base fluids. The study of platelet-shaped nanoparticles ($PbI_2 - PbMnI_2$) surrounded by a polymer matrix is discussed by Savchuk et al. [10]. Possessions of different forms of nanoparticles such as blades, bricks, platelets, spherical, and cylindrical on the enactment of tube heat exchangers have been scrutinized by Elias et al. [11]. Anselmo et al. [12] investigated the biological utilization of platelet-shaped particles to target vascular injuries and summarized that platelets particles have an ability to interact with vascular injury sites and have capability to marinate the vascular walls. Platelets nanoparticles are facilitated by their flexibility, shape, and composite device interactions. C CuO/H_2O forced convection nanofluid is explored under the inspiration of magnetic field by Sheikholeslami [13] and conferred the shapes effects of nanoparticles with the utilization of pedesis motion in the thermal stirring of nanofluids. Bahiraei and Monavari [14] glimpsed the hydro-thermal characteristics of microplate heat exchanger and studied nanoparticle shapes of blade, brick, platelet, and oblate spheroid. Here, it was deduced that platelet-shaped particles modify the performance of heat exchanger devices. Hayat et al. [15] examined the time-independent two-dimensional mixed-convection stream of micropolar fluid on nonlinear extendable device. Unsteady three-dimensional mixed-convection flow was considered by Hayat et al. [16] with the possessions of thermal conductivity and variable velocity on an exponentially elongated surface. Devi and Devi [17] numerically inspected the effects of Newtonian heating and Lorentz force on bidirectional movement of water-driven hybridized nanofluid with the thermal mixture of Cu and Al_2O_3 nanoparticles. From this consideration, it is examined that hybridized nanofluid delivers the better rate of heat transference than conventional nanofluids. Khan et al. [18] portrayed the magnetowater nanofluid with nonlinear thermal-radiation effects in mixed-convection stirring. Here, characteristics of heat transference in manifestation of convective boundary conditions were explored. Elsaid and Abdel [19] elaborated the mixed convection aspects of hybridized nanofluid $H_2O - Cu/Al_2O_3$ with the effects of adjustable temperature and thermal radiative flux. Here, it was depicted that thermal radiation increases the rate of heat transference by 12%–22% according to the ratio of tiny particles within the base fluid. The collective implications of magnetohydrodynamic (MHD) flow, thermal radiation, and Lorentz force produce a vibrant role in the improvement of film blowing, wire coating, fiber spinning, electron ramifications, nuclear weapons, polarization process, heat-conduction process, petroleum reservoirs. Hayat et al. [20] also deliberated MHD three-dimensional nanofluid with the features of nonlinear thermal radiation and partial slip on a permeable extending surface. Mahanthesh et al. [21] scrutinized the combined features of radiation and nonlinear thermal convection in three-dimensional boundary layer stream of Newtonian fluid, numerically.

Khashi'ie et al. [22] scrutinized the heat transference and flow properties of hybrid $Cu - Al_2O_3$/water nanofluid with the aspects of suction, joule-heating, and MHD on an elongating obstacle. Here, 10% of AlO_3 volume fraction with $3\% \leq Cu \leq 9\%$ volume fraction was picked to scrutinize the thermal performance of the system. Tlili et al. [23] considered the three-dimensional MHD stirring of hybridized nanofluid with aluminum containment of AA7072 and AA7075 in methanol liquid above an irregular thickness surface with the slip effects. Here, the influence of Lorentz force was estimated much less for the stirring of hybridized nanofluids as equated to conventional nanofluids. Abbas et al. [24] numerically explained the stirring of hybridized nanofluids on a stagnation point flow with an inclined magnetic field over a nonlinear elongating cylinder by utilizing the theory of Xue and Yamada-Ota models. The deviation in the temperature variation at the geometric surface is benevolent for several engineering and industrial solicitations. Yacob et al. [25] investigated numerically the Falkner-Skan problem for moving and static devices in a nanofluid with prescribed surface heat flux. Prakash and Devi [26] depicted hybridized nanofluid stirring Al_2O_3/Cu water with the aspects of hydromagnetic Lorentz force and prescribed surface temperature over a slandering expandable sheet. Here, it was deduced that hybridized nanofluid has better efficiency than nanofluid. Waini et al. [27] incorporated the hybridized nanofluid stirring and heat transference on a thin needle with prescribed surface heat flux. Dynamics of Cu/H_2O nanofluid with the consequences of prescribed surface temperature and prescribed heat flux have been scrutinized by Ahmed et al. [28]. Some recent novel contributions related with the applications of hybrid and nanofluids are made by researchers [29–34].

Under the circumstances of the above inclusive literature survey, it is perceived that much consideration has not been given to the stirring of hybridized nanofluid towards bidirectional elongating geometry. Therefore, the main theme of the current investigation is to examine the aspects of platelet-shaped nanoparticles (molybdenum disulfide and graphene oxide) for radiative water-driven hybridized nanofluid flow towards an unsteady bidirectional elongating obstacle with variable thermal constraints. Furthermore, the action of Lorentz force is also incorporated in the mathematical model. Apposite mathematical relations/symbols have been acted to renovate the leading equations into a dimensionless system, and then, numerical simulation is made via the Keller-Box method [35–37]. Finally, the chief results obtained through the current mathematical study are presented via different graphs/tables.

2. Mathematical Formulation

Cartesian configuration (as shown in Figure 1) is adopted in order to illuminate the unsteady fluid model for the

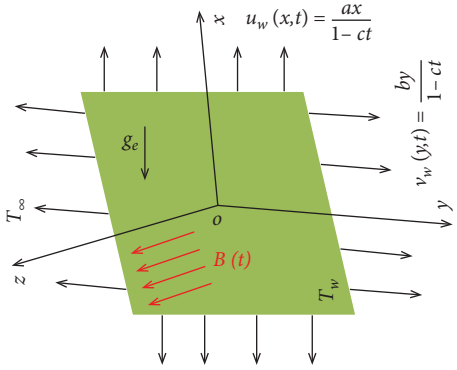

FIGURE 1: Cartesian configuration of the present model.

bidirectional stirring of water-driven hybridized nanofluid with nanoplatelets (molybdenum disulfide, MoS_2 *and* graphene oxide, GO). To incorporate the MHD (magnetohydrodynamics) process with variable strength B_0, mathematical relation of Lorentz force is used, however, to examine the impact of thermal radiation mathematical relation of Rosseland approximation is carried. The tiny particles are deliberated in thermal equilibrium under the response of mixed convection. Flow is laminar and incompressible by virtue of no-slip phenomenon. The velocity $u_w = ax/1 - ct; a > 0, c > 0$ is chosen along x-axis, and the velocity $v_w = by/1 - ct; b \geq 0$ is suggested along y-axis, but the space $0 < z < \infty$ is shielded by the hybridized nanofluid. Two categories of thermal conditions, i.e., VHF (variable heat flux) and VST (variable surface temperature), are functionalized to provide nonuniform temperature distribution at the device. Table 1 is made to recapitulate the thermophysical characteristics of water H_2O, molybdenum disulfide MoS_2, and graphene oxide GO.

In the persistence of the above suppositions with boundary layer theory, the transport rheology is established as

$$\frac{\partial u}{\partial x} + \frac{\partial v}{\partial y} + \frac{\partial w}{\partial z} = 0, \tag{1}$$

$$u\frac{\partial u}{\partial x} + v\frac{\partial u}{\partial y} + w\frac{\partial u}{\partial z} + \frac{\partial u}{\partial t} = \frac{\mu_{hnf}}{\rho_{hnf}}\left(\frac{\partial^2 u}{\partial z^2}\right) - \frac{\sigma_{hnf}}{\rho_{hnf}}B_0^2 u + \frac{g_e(\rho\beta)_{hnf}}{\rho_{hnf}}(T - T_\infty), \tag{2}$$

$$u\frac{\partial v}{\partial x} + v\frac{\partial v}{\partial y} + w\frac{\partial v}{\partial z} + \frac{\partial v}{\partial t} = \frac{\mu_{hnf}}{\rho_{hnf}}\left(\frac{\partial^2 v}{\partial z^2}\right) - \frac{\sigma_{hnf}}{\rho_{hnf}}B_0^2 v, \tag{3}$$

$$\frac{\partial T}{\partial t} + u\frac{\partial T}{\partial x} + v\frac{\partial T}{\partial y} + w\frac{\partial T}{\partial z} = \alpha_{hnf}\left(\frac{\partial^2 T}{\partial z^2}\right) - \frac{1}{(\rho C_p)_{hnf}}\frac{\partial q_{\text{rad}}}{\partial z}. \tag{4}$$

The thermal conditions and velocity field for equations (1)–(4) are conveyed as

$$z = 0: u = u_w(x,t) = \frac{ax}{1-ct}, v = v_w(y,t) = \frac{by}{1-ct}, w = 0, z \longrightarrow \infty: u \longrightarrow 0, v \longrightarrow 0,$$

$$\text{VST case}: z = 0: T = T_w(x,y,t) = T_\infty + T_0\left(\frac{x^r y^s}{1-ct}\right), z \longrightarrow \infty: T \longrightarrow T_\infty, \tag{5}$$

$$\text{VHF case}: z = 0: -k_f\left(\frac{\partial T}{\partial z}\right)_w = q_w(x,y,t) = T_1\left(\frac{x^r y^s}{1-ct}\right), z \longrightarrow \infty: T \longrightarrow T_\infty,$$

where g_e represents the gravitational pull, T illustrates the temperature at the surface, (u, v, w) entitle the velocity components along x-, y-, and z-directions, respectively, (r, s) are power indices, time factor is suggested by t, T_0 and T_1 are dimensional constants, μ_{hnf} is chosen to describe the effective viscosity of the hybridized mixture, k_{hnf} is taken to mark the thermal conductivity of the hybridized mixture, ρ_{hnf} is chosen to label the density of the hybridized mixture, α_{hnf} is selected to state the thermal diffusivity of the hybridized mixture, β_{hnf} is used to characterize the coefficient of thermal growth, $C_{p_{hnf}}$ designates the specific heat capacity, and σ_{hnf} is illustrated to express the stimulus of electrical conductivity of the hybridized nanofluid.

Table 1: Thermophysical features of molybdenum disulfide and graphene oxide nanoparticles with water as working fluid (Ref. [7]).

Thermophysical features	Base fluid	Nanoparticles	
	H_2O	MoS_2 (ψ_1)	GO (ψ_2)
Density (ρ): kg/m^3	997.1	5060	1800
Thermal conductivity (k): W/mK	0.613	904.4	5000
Specific heat (C_p): J/kgK	4179	397.21	717
Electrical conductivity (σ): S/m	0.005	2.09×10^4	6.30×10^7
Thermal expansion coefficient β:	21	2.8424×10^{-5}	2.84×10^{-4}
Prandtl number: Pr	6.20	-	-

The mathematical relations to familiarize the platelet-shaped nanoparticles for the present evolution of hybridized nanomaterial are discussed as

$$
\begin{aligned}
(\rho\beta)_{hnf} &= \psi_1(\rho\beta)_{p1} + \psi_2(\rho\beta)_{p2} + (1-\psi_1-\psi_2)(\rho\beta)_f,\\
\rho_{hnf} &= \psi_1\rho_{p1} + \psi_2\rho_{p2} + (1-\psi_1-\psi_2)\rho_f,\\
\left(\rho C_p\right)_{hnf} &= \psi_1\left(\rho C_p\right)_{p1} + \psi_2\left(\rho C_p\right)_{p2} + (1-\psi_1-\psi_2)\left(\rho C_p\right)_f,\\
\frac{k_{hnf}}{k_{bf}} &= \frac{\left(k_{p2}+4.72k_{bf}\right)+4.72\psi_2\left(k_{p2}-k_{bf}\right)}{\left(k_{p2}+4.72k_{bf}\right)-\psi_2\left(k_{p2}-k_{bf}\right)},\\
\frac{k_{bf}}{k_f} &= \frac{\left(k_{p1}+4.72k_f\right)+4.72\psi_1\left(k_{p1}-k_f\right)}{\left(k_{p1}+4.72k_f\right)-\psi_1\left(k_{p1}-k_f\right)},\\
\frac{\sigma_{hnf}}{\sigma_{bf}} &= 1+\frac{3\left(\sigma_{p2}/\sigma_{bf}-1\right)\psi_2}{\sigma p_2/\sigma_{bf}+2-\left(\sigma_{p2}/\sigma_{bf}-1\right)\psi_2},\\
\frac{\sigma_{bf}}{\sigma_f} &= 1+\frac{3\left(\sigma_{p1}/\sigma_f-1\right)\psi_1}{\sigma_{p1}/\sigma_f+2-\left(\sigma_{p1}/\sigma_f-1\right)\psi_1},\\
\alpha_{hnf} &= \frac{k_{hnf}}{\left(\rho C_p\right)_{hnf}},\\
\frac{\mu_{hnf}}{\mu_{bf}} &= 1+37.1\psi_2+612.6\psi_2^2,\\
\frac{\mu_{bf}}{\mu_f} &= 1+37.1\psi_1+612.6\psi_1^2,
\end{aligned}
\tag{6}
$$

where quantities of molybdenum disulfide and graphene oxide tiny particles are expressed through ψ_1 and ψ_2, respectively.

The expression for radiative heat transaction is composed as (Ref. [21])

$$
q_{\text{rad}} = -\frac{16\sigma^*}{3k^*}T^3\frac{\partial T}{\partial z}, \tag{7}
$$

where k^* is allotted for the mean-immersion coefficient, and σ^* implied for the Stefan-Boltzmann constant. It is worthy to mention here that T^3 in equation (7) was prolonged about T_∞ in most literature related with thermal radiation; however, in the current scenario, this has been escaped to get more convincing and significant outcomes. Thus, the manifestation for thermal radiation in equation (7) is nonlinear, and it yields the effect of nonlinear thermal radiation for present flow exploration.

The set of equations adopted to nondimensionalize the present mathematical formulation is written as

$$
\begin{aligned}
u &= \frac{\text{ax}}{1-\text{ct}}f'(\eta),\ v = \frac{\text{ay}}{1-\text{ct}}g'(\eta), w\\
&= -\left(\frac{a\vartheta_f}{1-\text{ct}}\right)^{1/2}[f(\eta)+g(\eta)], \eta = \left(\frac{a}{\vartheta_f(1-\text{ct})}\right)^{1/2}z,
\end{aligned}
\tag{8}
$$

$$
\begin{aligned}
\text{VST case}: \theta(\eta) &= \frac{T(x,y,z,t)-T_\infty}{T_w(x,y,t)-T_\infty},\\
\text{VHF case}: T-T_\infty &= \frac{T_1}{k_f}\left(\frac{\vartheta_f}{a(1-ct)}\right)^{1/2}x^r y^s\phi(\eta).
\end{aligned}
\tag{9}
$$

With the incorporation of equations (8) and (9), principal equations become

$$
\varepsilon_1 f''' + (f+g)f'' - f'^2 - S\left(f' + \frac{\eta}{2}f''\right) - \varepsilon_2 M^2 f' + \varepsilon_4\lambda_t\theta = 0, \tag{10}
$$

$$
\varepsilon_1 g''' + (f+g)g'' - g'^2 - S\left(g' + \frac{\eta}{2}g''\right) - \varepsilon_2 M^2 g' = 0, \tag{11}
$$

$$
\begin{aligned}
&\text{VST case}: \varepsilon_3\frac{d}{d\eta}\left[\left(1+R_d\left(1+(\theta_w-1)\theta\right)^3\right)\theta'\right]\\
&+\text{Pr}\left(\frac{(f+g)\theta' - (rf'+sg')\theta}{-S\left(\theta+(\eta/2)\theta'\right)}\right) = 0,
\end{aligned}
\tag{12}
$$

$$
\begin{aligned}
&\text{VHF case}: \varepsilon_3\frac{d}{d\eta}\left[\left(1+R_d\left(1+(\theta_w-1)\phi\right)^3\right)\phi'\right]\\
&+\text{Pr}\left(\frac{(f+g)\phi' - (rf'+sg')\phi}{-S\left(\phi+(\eta/2)\phi'\right)}\right) = 0.
\end{aligned}
\tag{13}
$$

With boundary restrictions,

$$
\begin{aligned}
&f(0)+g(0)=0,\ f'(0)=1,\ g'(0)=\alpha, \theta(0)=1, \phi'(0)=-1,\\
&f'(\infty)\longrightarrow 0, g'(\infty)\longrightarrow 0, \theta(\infty)\longrightarrow 0, \phi(\infty)\longrightarrow 0.
\end{aligned}
\tag{14}
$$

The current model can be reduced to unidirectional flow by considering $\alpha = 0$ and reduced to axisymmetric flow by adopting $\alpha = 1.0$. Here, $\lambda_t = \text{Gr}/(\text{Re}_x)^2$ illustrates the buoyancy factor, $Gr = \beta_f g_e(T_w - T_\infty)x^3/\vartheta_f^2$ represents the Grashof number, $\theta_w = T_w/T_\infty$ symbolized for the temperature constraint with $T_w > T_\infty$, Hartman number is documented by $M = (\sigma_f/a\rho_f)^{1/2}B_0$, unsteadiness is stated by

$S = c/a$, stretching effect is expressed by $\alpha = b/a$, Prandtl number is specified by $\mathrm{Pr} = \upsilon_f/\alpha_f$, $R_d = 16\sigma^*/3k^*k_fT_\infty^3$ is the radiation factor, and $(\varepsilon_1, \varepsilon_2, \varepsilon_3, \varepsilon_4)$ are the relationships for current hybridized mixture and are elaborated as

$$\begin{aligned}
\varepsilon_1 &= \frac{\left(1+37.1\psi_2+612.6\psi_2^2\right)\left(1+37.1\psi_1+612.6\psi_1^2\right)}{\left(\psi_1\rho_{p1}/\rho_f+\psi_2\rho_{p2}/\rho_f+(1-\psi_1-\psi_2)\right)},\\
\varepsilon_2 &= \frac{\left(1+3\left(\sigma_{p2}/\sigma_{bf}-1\right)\psi_2/\sigma_{p2}/\sigma_{bf}+2-\left(\sigma_{p2}/\sigma_{bf}-1\right)\psi_2\right)\left(1+3\left(\sigma_{p1}/\sigma_f-1\right)\psi_1/\sigma_{p1}/\sigma_f+2-\left(\sigma_{p1}/\sigma_f-1\right)\psi_1\right)}{\psi_1\rho_{p1}/\rho_f+\psi_2\rho_{p2}/\rho_f+(1-\psi_1-\psi_2)},\\
\varepsilon_3 &= \frac{\left(\left(k_{p2}+4.72k_{bf}\right)+4.72\psi_2\left(k_{p2}-k_{bf}\right)/\left(k_{p2}+4.72k_{bf}\right)-\psi_2\left(k_{p2}-k_{bf}\right)\right)\left(\left(k_{p1}+4.72k_f\right)+4.72\psi_1\left(k_{p1}-k_f\right)/\left(k_{p1}+4.72k_f\right)-\psi_1\left(k_{p1}-k_f\right)\right)}{\psi_1\left(\rho C_p\right)_{p1}/\left(\rho C_p\right)_f+\psi_2\left(\rho C_p\right)_{p2}/\left(\rho C_p\right)_f+(1-\psi_1-\psi_2)},\\
\varepsilon_4 &= \frac{\left(\psi_1(\rho\beta)_{p1}/(\rho\beta)_f+\psi_2(\rho\beta)_{p2}/(\rho\beta)_f+(1-\psi_1-\psi_2)\right)}{\left(\psi_1\rho_{p1}/\rho_f+\psi_2\rho_{p2}/\rho_f+(1-\psi_1-\psi_2)\right)}.
\end{aligned} \tag{15}$$

The most captivating quantity for thermal processes is the local Nusselt number and is communicated in the form of Reynolds's number $\mathrm{Re}_x = \mathrm{xu}_w/\vartheta_f$ as

$$Nu = \begin{cases} -\dfrac{x\left[k_{hnf}\left(\partial T/\partial z\right)_{z=0}+16\sigma^*/3k^*\left(T^3\partial T/\partial z\right)_{z=0}\right]}{k_f\left(T_w-T_\infty\right)} & \text{(VST case)} \\ -\dfrac{x\left[k_{hnf}\left(\partial T/\partial z\right)_{z=0}+16\sigma^*/3k^*\left(T^3\partial T/\partial z\right)_{z=0}\right]}{k_f\left(T-T_\infty\right)} & \text{(VHF case)} \end{cases},$$

$$\frac{-1}{\mathrm{Re}_x^{2}}\,\mathrm{Nu} = \begin{cases} -\dfrac{k_{hnf}}{k_f}\left[1+R_d\left(\theta_w\right)^3\right]\theta'(0)\,\text{(VST case)} \\ \dfrac{k_{hnf}}{k_f}\left(1+R_d\left(\phi(0)\left(\theta_w-1\right)+1\right)^3\right)\dfrac{1}{\phi(0)}\ \text{(VHF case)} \end{cases}. \tag{16}$$

3. Keller-Box Simulation

This numerical scheme introduced by Keller can be used in other physical models. This numerical technique has a quick convergence capability than other numerical techniques (such as shooting method, RK-method, and RKF-45 method). The Keller-Box method can be applied to solve those ODEs or PDEs whose linearization is possible. Keller-Box method has the following sequence of steps, and its coding procedure is described in Figure 2.

(i) Transformation process for second and higher-order differential equations into first-order differential equations

(ii) Completion of discretization scheme using central difference approximations

(iii) Transformation of the differential system into difference system of equations using the above discretization scheme

(iv) Application of Newton Raphson method in order to linearize the difference equations system

(v) Formation of the matrix-vector form of the system

(vi) Solution of the matrix-vector form by using LU-decomposition tactic

Assume the grid points $[\eta_0, \eta_1, \eta_2, \ldots \eta_N]$, where $\eta_0 = 0$, $\eta_N = \eta_{\max} < \infty$, and intermediate steps have not same length. To attain first approximation, we chose $\eta_0 = 0, \eta_\infty = 15, n_p = 600, h = \eta_\infty - \eta_0/n_p$, and we got the required result, i.e., $\varepsilon = 10^{-5}$ is achieved by varying the value of n_p (the numbers of grid points) with the reduction in the value of h (step size). Table 2 explores the convergence

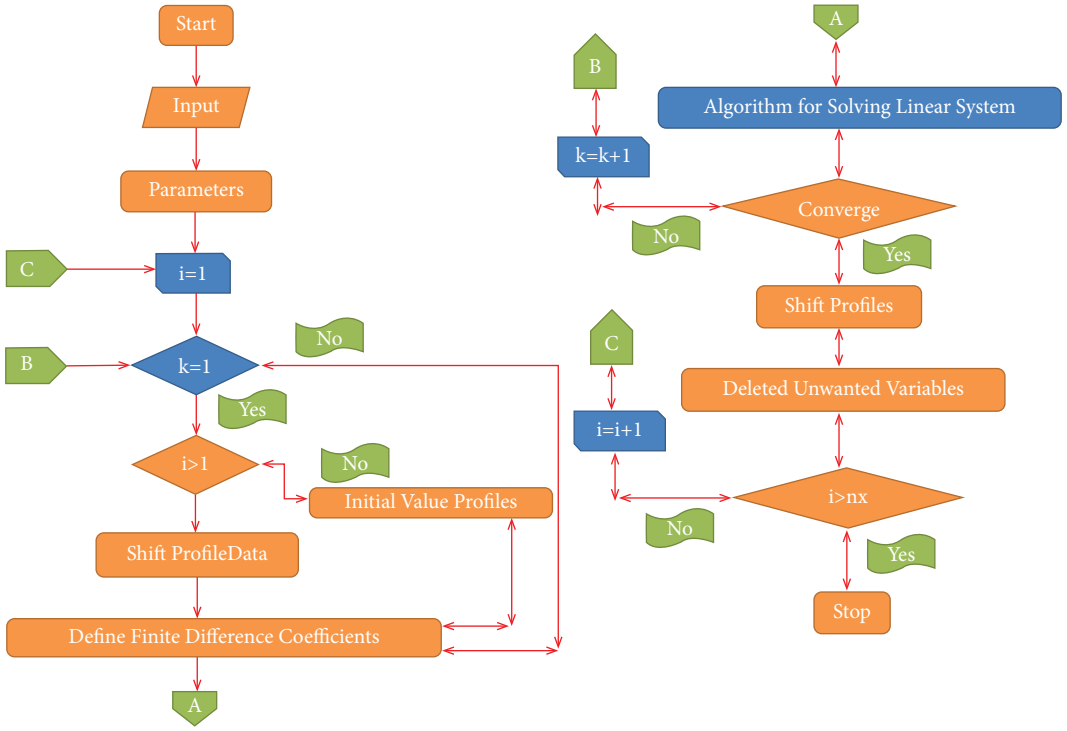

Figure 2: Coding procedure of Keller-Box method.

Table 2: Convergence table for VST case under the control of $\alpha = S = M = 0.5, \lambda = 0.2, r = s = 1.0, \psi_1 = 0.01, \psi_2 = 0.02, R_d = 0.4, \theta_w = 1.1, \lambda_t = 0.2$.

n_p	$-f''(0)$	$-g''(0)$	$-\theta'(0)$
600	0.8007	0.36853	2.80524
1200	0.8007	0.36853	2.80505
1800	0.8007	0.36853	2.80501
2400	0.8007	0.36853	2.8050
3000	0.8007	0.36853	2.80499
3600	0.8007	0.36853	2.80499

analysis for the present simulation under the regulation of the involved engineering parameters, i.e., $\alpha = S = M = 0.5, \lambda = 0.2, r = s = 1.0, \psi_1 = 0.01, \psi_2 = 0.02, R_d = 0.4, \theta_w = 1.1, \lambda_t = 0.2$ for VST case. The first row of Table 2 is obtained by selecting $\eta_0 = 0, \eta_\infty = 15, n_p = 600$ in order to start the numerical solution with the defined accuracy, and then, the value of n_p is increased uniformly up to thirty-six hundred. It is noticed in Table 2 that $n_p = 600$ provides the stable solution for equations (10) and (11), whereas $n_p = 3000$ provides the stable solution for equation (12) under the control of VST modulation. However, the solution is provided up to $n_p = 3600$ to achieve the stability of the numerical solution.

Table 3 explores the convergence analysis for present simulation under the regulation of the involved engineering parameters, i.e., $\alpha = S = M = 0.5, \lambda = 0.2, r = s = 1.0, \psi_1 = 0.01, \psi_2 = 0.02, R_d = 0.4, \theta_w = 1.1, \lambda_t = 0.2$ for VHF case. The first row of Table 3 is obtained by selecting $\eta_0 = 0, \eta_\infty = 15, n_p = 600$ in order to start the numerical solution with the defined accuracy, and then, the value of n_p is increased gradually up to three thousand. It is noticed in Table 3 that $n_p = 600$ provides the stable solution for equations (10) and (11), whereas $n_p = 2400$ provides the stable solution for equation (12) under the control of VHF modulation. However, the solution is provided up to $n_p = 3000$ to achieve the stability of the numerical solution.

4. Results and Discussion

The exposures of newly obtained involved parameters, i.e., temperature maintaining indices r& s and temperature ratio T_w on thermal setups [$\theta(\eta)$ (for VST case) and $\phi(\eta)$ (for VHF case)] through present mathematical modeling are elaborated via Figures 3(a)–5(b). Figure 3(a) is used to predict the temperature fluctuation under VST modulation, whereas Figure 3(b) is plotted to predict the temperature fluctuation under VHF modulation for $r = -2, -1, 0, 1, 2$. It is concluded through Figure 3(a) that escalating value of r

Table 3: Convergence table for VHF case under the control of $\alpha = S = M = 0.5, \lambda = 0.2, r = s = 1.0, \psi_1 = 0.01, \psi_2 = 0.02, R_d = 0.4, \theta_w = 1.1, \lambda_t = 0.2$.

n_p	$-f''(0)$	$-g''(0)$	$\phi(0)$
600	0.81169	0.36843	0.343419
1200	0.81169	0.36843	0.343440
1800	0.81169	0.36843	0.343444
2400	0.81169	0.36843	0.343446
3000	0.81169	0.36843	0.343446

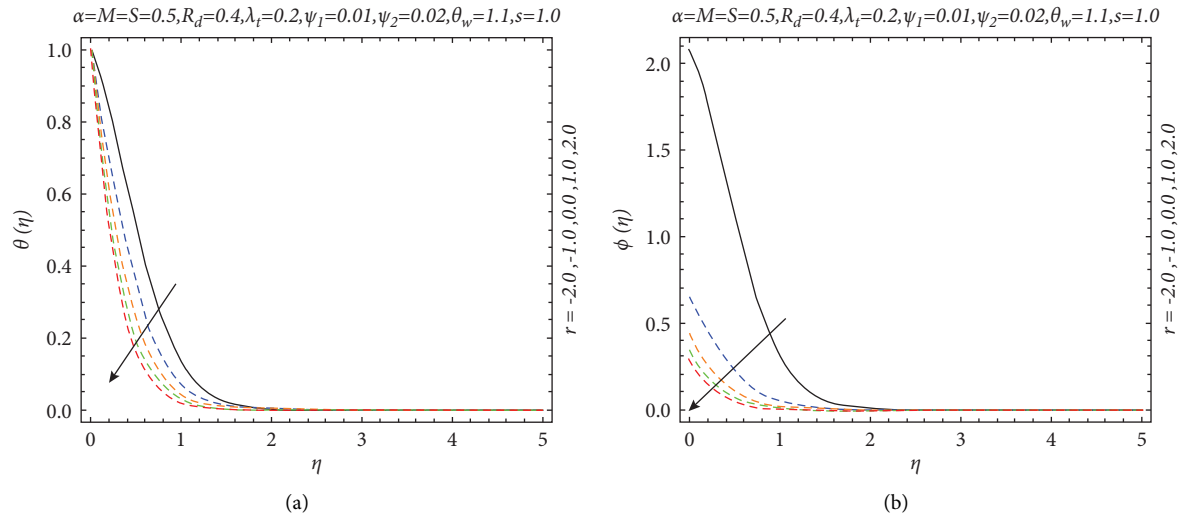

Figure 3: (a, b): Temperature against the variation of the index r for VST case (plot a) and for VHF case (plot b).

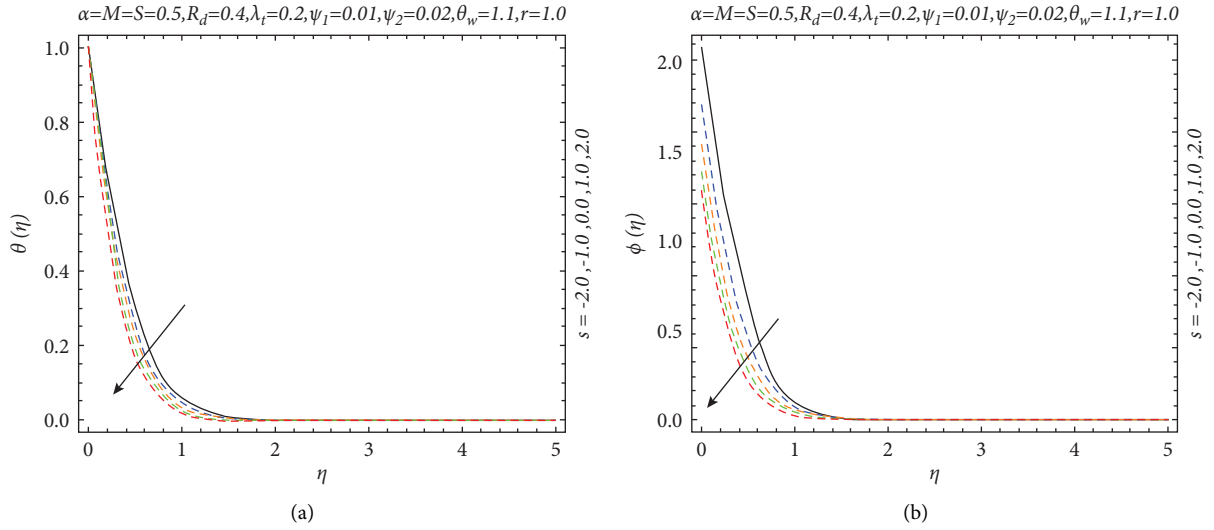

Figure 4: (a, b): Temperature against the variation of the index s for VST case (plot a) and for VHF case (plot b).

reduces the temperature of the nanomaterial. For negative values of r, temperature of the material is observed very high as compared to the positive values of r. Moreover, the width of thermal layer is higher for consecutive negative amounts of r as compared to the consecutive positive amounts of r. The behaviour of the index r on thermal setup for VHF modulation is discussed via Figure 3(b). It is noticed through Figure 3(b) that temperature reduces with the higher values of r, but the temperature is detected higher for VHF case as compared to VST case for smaller values of r. Figure 4(a) is plotted to discuss the temperature fluctuation under VST modulation, whereas Figure 4(b) is used to predict the temperature fluctuation under VHF modulation for second index $s = -2, -1, 0, 1, 2$. It is concluded through Figure 4(a) that escalating value of s reduces the temperature of the nanomixture.

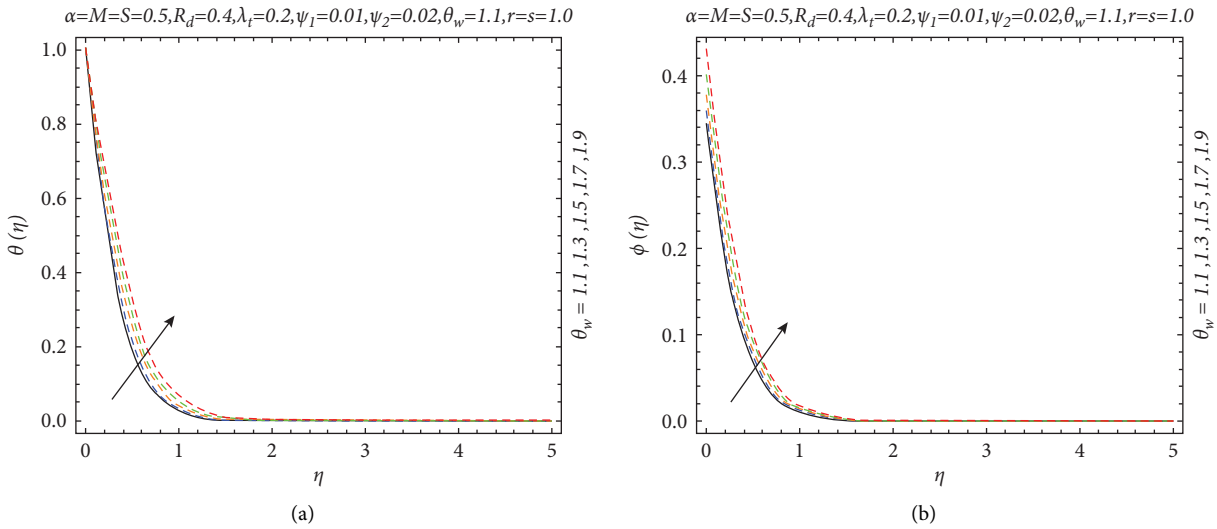

Figure 5: (a, b): Temperature against the variation of radiation factor θ_w for VST case (plot a) and for VHF case (plot b).

Table 4: Involvement of solid volume fractions ψ_1 and ψ_2 for $\alpha = S = M = 0.5, \lambda = 0.2, r = s = 1.0, R_d = 0.4, \theta_w = 1.1, \lambda_t = 0.2$.

Nanoparticles volume fractions		Nusselt numbers	
ψ_1	ψ_2	VHF case	VST case
0.02	0.01	4.954664	5.070091
0.04	0.01	5.227523	5.357409
0.06	0.01	5.478023	5.620055
0.01	0.02	4.96080	5.07644
0.01	0.04	5.244287	5.374786
0.01	0.06	5.504457	5.647509

Tables 5: Involvement of λ_t (buoyancy factor), R_d (radiation factor), and S (unsteady parameter) for $\alpha = M = 0.5, \lambda = 0.2, r = s = 1.0, \psi_1 = 0.01, \psi_2 = 0.02, \theta_w = 1.1$.

Parameters			Nusselt numbers	
λ_t	R_d	S	VHF case	VST case
0.2	0.4	0.5	4.9608	5.07644
0.4	0.4	0.5	4.961706	5.079255
0.6	0.4	0.5	4.96261	5.082058
0.2	0.8	0.5	5.631413	5.813119
0.2	1.2	0.5	6.229136	6.450445
0.2	1.6	0.5	6.773362	7.017367
0.2	0.4	1.0	5.294724	5.422095
0.2	0.4	1.5	5.621479	5.760534
0.2	0.4	2.0	5.939044	6.089599

For negative values of s, temperature of the material is observed very high as compared to the positive values of s. Moreover, the width of thermal layer is higher for consecutive negative amounts of s as compared to the consecutive positive amounts of s. The behaviour of the index s on thermal setup for VHF modulation is discussed via Figure 4(b). It is noticed through Figure 4(b) that temperature reduces with the higher values of s, but the temperature is detected higher for VHF case as compared to VST case for smaller values of r. The width of thermal layer in the case of s is much smaller than the width of thermal layer for the index r. Physically, the stretching ratio α is higher for x-direction as compared to y-direction. As r represents the index with respect to x-direction and s represents the index in the y-direction, so the above spectacular outcomes are obtained which are highly useful in many thermal engineering systems involved in industry and manufacturing. Figure 5(a) describes the impact of θ_w on thermal setup for VST case, whereas Figure 5(b) illustrates the importance of θ_w on thermal setup for VHF case. Positive tendencies in the temperature fluctuation for both VST and VHF cases are achieved with the escalation in the choice of θ_w from 1.1 to 1.9. The worth of temperature is detected high for VST modulation as compared to VHF modulation. Table 4 enlightens the involvement of solid volume fractions ψ_1 and ψ_2 on local Nusselt numbers under the control of the involved engineering parameters, i.e., $\alpha = S = M = 0.5, \lambda = 0.2, r = s = 1.0, R_d = 0.4, \theta_w = 1.1, \lambda_t = 0.2$ for both VST and VHF cases. From Table 4, it is established that increasing values of ψ_1 and ψ_2, and local Nusselt numbers are enhanced in both VHF and VST cases. Table 5 discloses the impact of λ_t (buoyancy factor), R_d (radiation factor), and S (unsteady parameter) on Nusselt numbers under the influence of $\alpha = M = 0.5, \lambda = 0.2, r = s = 1.0, \psi_1 = 0.01, \psi_2 = 0.02, \theta_w = 1.1$. It is noticed through Table 5 that increasing values of buoyancy factor, radiation factor, and unsteady parameter enhance the local Nusselt numbers for both VHF and VST cases.

5. Conclusions

This study gives the mathematical exploration for unsteady bidirectional dynamics of nanoplatelets (MoS_2 + GO) under variable thermal aspects. Nonlinear thermal radiation, magnetohydrodynamics, and mixed convection features have also been studied to make the investigation more impactful. Solution is made through Keller-Box technique, and significant observations are itemized as follows:

(i) Temperature profile is enhanced with the escalation of θ_w, and it is reduced with appreciations of thermal indices (r, s)

(ii) Nusselt number is observed higher for VHF case than VST case

(iii) Thermal performance of the system is enhanced with the suspension of nanoplatelets (molybdenum disulfide and graphene oxide) in water

The outcomes of the present investigation are helpful in the development of solar collector, coating a sheet with hybrid nanomaterials, improvement of the thermal system used in industry, etc. In future, this work can be extended with non-Newtonian hybrid nanofluids and ternary hybrid nanofluids.

Data Availability

The raw data supporting the conclusions of this article will be made available by the corresponding author without undue reservation.

Conflicts of Interest

The authors declare that there are no conflicts of interest.

Authors' Contributions

All authors contributed equally to this work.

References

[1] O. D. Makinde and A. Aziz, "Boundary layer flow of a nanofluid past a stretching sheet with a convective boundary condition," *International Journal of Thermal Sciences*, vol. 50, no. 7, pp. 1326–1332, 2011.

[2] I. Waini, A. Ishak, T. Groşan, and I. Pop, "Mixed convection of a hybrid nanofluid flow along a vertical surface embedded in a porous medium," *International Communications in Heat and Mass Transfer*, vol. 114, Article ID 104565, 2020.

[3] T. Gul, A. Khan, M. Bilal et al., "Magnetic dipole impact on the hybrid nanofluid flow over an extending surface," *Scientific Reports*, vol. 10, no. 1, pp. 8474–8513, 2020.

[4] I. Waini, A. Ishak, and I. Pop, "Transpiration effects on hybrid nanofluid flow and heat transfer over a stretching/shrinking sheet with uniform shear flow," *Alexandria Engineering Journal*, vol. 59, no. 1, pp. 91–99, 2020.

[5] A. Moghadassi, E. Ghomi, and F. Parvizian, "A numerical study of water based Al2O3 and Al2O3–Cu hybrid nanofluid effect on forced convective heat transfer," *International Journal of Thermal Sciences*, vol. 92, pp. 50–57, 2015.

[6] S. S. Ghadikolaei, M. Yassari, H. Sadeghi, K. Hosseinzadeh, and D. D. Ganji, "Investigation on thermophysical properties of Tio2–Cu/H2O hybrid nanofluid transport dependent on shape factor in MHD stagnation point flow," *Powder Technology*, vol. 322, pp. 428–438, 2017.

[7] B. Ali, R. A. Naqvi, D. Hussain, O. M. Aldossary, and S. Hussain, "Magnetic rotating flow of a hybrid nano-materials Ag-MoS2 and Go-MoS2 in C2H6O2-H2O hybrid base fluid over an extending surface involving activation energy: FE simulation," *Mathematics*, vol. 8, no. 10, p. 1730, 2020.

[8] A. U. Yahya, N. Salamat, W. H. Huang, I. Siddique, S. Abdal, and S. Hussain, "Thermal charactristics for the flow of Williamson hybrid nanofluid (MoS2 + ZnO) based with engine oil over a streched sheet," *Case Studies in Thermal Engineering*, vol. 26, Article ID 101196, 2021.

[9] M. Arif, P. Kumam, D. Khan, and W. Watthayu, "Thermal performance of GO-MoS2/engine oil as Maxwell hybrid nanofluid flow with heat transfer in oscillating vertical cylinder," *Case Studies in Thermal Engineering*, vol. 27, Article ID 101290, 2021.

[10] A. I. Savchuk, V. I. Fediv, Y. O. Kandyba, T. A. Savchuk, I. D. Stolyarchuk, and P. I. Nikitin, "Platelet-shaped nanoparticles of PbI2 and PbMnI2 embedded in polymer matrix," *Materials Science and Engineering: C*, vol. 19, no. 1-2, pp. 59–62, 2002.

[11] M. M. Elias, M. Miqdad, I. M. Mahbubul et al., "Effect of nanoparticle shape on the heat transfer and thermodynamic performance of a shell and tube heat exchanger," *International Communications in Heat and Mass Transfer*, vol. 44, pp. 93–99, 2013.

[12] A. C. Anselmo, C. L. Modery-Pawlowski, S. Menegatti et al., "Platelet-like nanoparticles: mimicking shape, flexibility, and surface biology of platelets to target vascular injuries," *ACS Nano*, vol. 8, no. 11, Article ID 11243, 2014.

[13] M. Sheikholeslami, "Magnetic field influence on CuO–H2O nanofluid convective flow in a permeable cavity considering various shapes for nanoparticles," *International Journal of Hydrogen Energy*, vol. 42, no. 31, Article ID 19611, 2017.

[14] M. Bahiraei and A. Monavari, "Thermohydraulic characteristics of a micro plate heat exchanger operated with nanofluid considering different nanoparticle shapes," *Applied Thermal Engineering*, vol. 179, Article ID 115621, 2020.

[15] T. Hayat, Z. Abbas, and T. Javed, "Mixed convection flow of a micropolar fluid over a non-linearly stretching sheet," *Physics Letters A*, vol. 372, no. 5, pp. 637–647, 2008.

[16] T. Hayat, M. I. Khan, M. Farooq, N. Gull, and A. Alsaedi, "Unsteady three-dimensional mixed convection flow with variable viscosity and thermal conductivity," *Journal of Molecular Liquids*, vol. 223, pp. 1297–1310, 2016.

[17] S. S. U. Devi and S. A. Devi, "Numerical investigation of three-dimensional hybrid Cu–Al2O3/water nanofluid flow over a stretching sheet with effecting Lorentz force subject to Newtonian heating," *Canadian Journal of Physics*, vol. 94, no. 5, pp. 490–496, 2016.

[18] M. I. Khan, M. Waqas, T. Hayat, A. Alsaedi, and M. I. Khan, "Significance of nonlinear radiation in mixed convection flow of magneto Walter-B nanoliquid," *International Journal of Hydrogen Energy*, vol. 42, no. 42, Article ID 26408, 2017.

[19] E. M. Elsaid and M. S. Abdel-Wahed, "Mixed convection hybrid-nanofluid in a vertical channel under the effect of thermal radiative flux," *Case Studies in Thermal Engineering*, vol. 25, Article ID 100913, 2021.

[20] T. Hayat, M. Imtiaz, A. Alsaedi, and M. A. Kutbi, "MHD three-dimensional flow of nanofluid with velocity slip and nonlinear thermal radiation," *Journal of Magnetism and Magnetic Materials*, vol. 396, pp. 31–37, 2015.

[21] B. Mahanthesh, B. J. Gireesha, G. T. Thammanna, S. A. Shehzad, F. M. Abbasi, and R. S. R. Gorla, "Nonlinear convection in nano Maxwell fluid with nonlinear thermal radiation: a three-dimensional study," *Alexandria Engineering Journal*, vol. 57, no. 3, pp. 1927–1935, 2018.

[22] N. S. Khashi'ie, N. M. Arifin, R. Nazar, E. H. Hafidzuddin, N. Wahi, and I. Pop, "Magnetohydrodynamics (MHD) axisymmetric flow and heat transfer of a hybrid nanofluid past a

radially permeable stretching/shrinking sheet with Joule heating," *Chinese Journal of Physics*, vol. 64, pp. 251–263, 2020.

[23] I. Tlili, H. A. Nabwey, G. P. Ashwinkumar, and N. Sandeep, "3-D magnetohydrodynamic AA7072-AA7075/methanol hybrid nanofluid flow above an uneven thickness surface with slip effect," *Scientific Reports*, vol. 10, no. 1, pp. 4265–4313, 2020.

[24] N. Abbas, S. Nadeem, A. Saleem, M. Y. Malik, A. Issakhov, and F. M. Alharbi, "Models base study of inclined MHD of hybrid nanofluid flow over nonlinear stretching cylinder," *Chinese Journal of Physics*, vol. 69, pp. 109–117, 2021.

[25] N. A. Yacob, A. Ishak, R. Nazar, and I. Pop, "Falkner–Skan problem for a static and moving wedge with prescribed surface heat flux in a nanofluid," *International Communications in Heat and Mass Transfer*, vol. 38, no. 2, pp. 149–153, 2011.

[26] M. Prakash and S. S. U. Devi, "Hydromagnetic hybrid Al2O3-Cu/water nanofluid flow over a slendering stretching sheet with prescribed surface temperature," *Asian Journal of Research in Social Sciences and Humanities*, vol. 6, no. 9, pp. 1921–1936, 2016.

[27] I. Waini, A. Ishak, and I. Pop, "Hybrid nanofluid flow and heat transfer past a vertical thin needle with prescribed surface heat flux," *International Journal of Numerical Methods for Heat and Fluid Flow*, vol. 29, no. 12, pp. 4875–4894, 2019.

[28] I. Ahmad, M. Faisal, and T. Javed, "Dynamics of copper–water nanofluid with the significance of prescribed thermal conditions," *Heat Transfer*, vol. 50, no. 5, pp. 4248–4263, 2021.

[29] F. Ali, T. Arun Kumar, K. Loganathan et al., "Irreversibility analysis of cross fluid past a stretchable vertical sheet with mixture of Carboxymethyl cellulose water based hybrid nanofluid," *Alexandria Engineering Journal*, 2022.

[30] S. Chandrasekaran, M. Satyanarayana Gupta, S. Jangid, K. Loganathan, B. Deepa, and D. K Chaudhary, "Unsteady radiative Maxwell fluid flow over an expanding sheet with sodium alginate water-based copper-graphene oxide hybrid nanomaterial: an application to solar aircraft," *Advances in Materials Science and Engineering*, vol. 2022, no. 1, 16 pages, Article ID 8622510, 2022.

[31] M. Faisal, F. Mabood, and I. A. Badruddin, "On numerical analysis of hydromagnetic radiative Jeffery nanofluid flow by variable thickness surface with activation energy and unsteadiness aspects," *Waves in Random and Complex Media*, pp. 1–19, 2022.

[32] S. U. Khan and H. M. Ali, "Swimming of gyrotactic microorganisms in unsteady flow of Eyring Powell nanofluid with variable thermal features: some bio-technology applications," *International Journal of Thermophysics*, vol. 41, no. 11, pp. 159–219, 2020.

[33] R. Prabakaran, S. Eswaramoorthi, K. Loganathan, and I. E. Sarris, "Investigation on thermally radiative mixed convective flow of carbon nanotubes/Al_2O_3 nanofluid in water past a stretching plate with joule heating and viscous dissipation," *Micromachines*, vol. 13, no. 9, p. 1424, 2022.

[34] S. Saleem, I. L. Animasaun, S. J. Yook, Q. M. Al-Mdallal, N. A. Shah, and M. Faisal, "Insight into the motion of water conveying three kinds of nanoparticles shapes on a horizontal surface: significance of thermo-migration and Brownian motion," *Surfaces and Interfaces*, vol. 30, Article ID 101854, 2022.

[35] W. Farooq, A. Abbasi, K. Al-Khaled et al., "Thermal aspect of boron nitride nanotubes (BNNT) and multiwall carbon nanotubes (MWCNT) with distinct physical features: Keller Box simulations," *ZAMM-Journal of Applied Mathematics and Mechanics/Zeitschrift für Angewandte Mathematik und Mechanik*, Article ID e202100560, 2022.

[36] N. M. Sarif, M. Z. Salleh, and R. Nazar, "Numerical solution of flow and heat transfer over a stretching sheet with Newtonian heating using the Keller box method," *Procedia Engineering*, vol. 53, pp. 542–554, 2013.

[37] A. Abbasi, K. Al-Khaled, M. I. Khan et al., "Electro-osmotic flow of Prandtl nanofluids with thermal and solutal slip flow constraints: Keller Box simulations," *Arabian Journal for Science and Engineering*, vol. 47, no. 7, pp. 8439–8456, 2022.